Supporting information

Unravelling the intrinsic synergy between Pt and MnO_x supported on porous calcium silicate during toluene oxidation

Ziqiang Wang [a,b,c], Zhifei Hao [a,b,c,*], Yinmin Zhang [a,b,c], Yongfeng Zhang [a,b,c,*]

[a] College of Chemical Engineering, Inner Mongolia University of Technology, Hohhot, 010051, China,

[b] Inner Mongolia Key Laboratory of Efficient Cyclic Utilization of Coal-Based Solid Waste, Hohhot, 010051, China,

[c] Key Laboratory of Resource Circulation at Universities of Inner Mongolia Autonomous Region, Hohhot, 010051, China,

[*]Corresponding author

Email address: haozhifei@imut.edu.cn (Z. Hao); environzyf@sina.com (Y. Zhang)

1. Experimental Section

1.1 Catalyst preparation

1.0g PCS support and a certain amount of $Mn(CH_3COO)_2 \cdot 4H_2O$ were dissolved in appropriate ultra-pure water respectively, and then the $Mn(CH_3COO)_2 \cdot 4H_2O$ solution was added dropwise into PCS solution under the condition of constant stirring. Finally, added 0.267 ml $H_2PtCl_6 \cdot 6H_2O$ aqueous solution with the concentration was 3.75 mg/ml, the mixture was then put into a water bath at 70°C with magnetic stirring until all the water evaporation. The resulting solid products were calcined at 400°C for 3h in air atmosphere with the heating rate of 5°C/min. Adjusting the amount of $Mn(CH_3COO)_2 \cdot 4H_2O$ to vary the Mn load. The final catalysts were denoted as 0.1Pt-*X*MnO_x/PCS (*X*=0.5, 1, 5, 10, 15, represents the load of Mn). In addition, the 0.1Pt/PCS and 5MnO_x/PCS were prepared according to the above method without adding $Mn(CH_3COO)_2 \cdot 4H_2O$ and $H_2PtCl_6 \cdot 6H_2O$, respectively.

The Manganese acetate tetrahydrate ($Mn(CH_3COO)_2 \cdot 4H_2O$, 99%) and Chloroplatinic acid hexahydrate ($H_2PtCl_6 \cdot 6H_2O$, Pt content ≥ 37.5%) were A.R., and purchased from Aladdin.

1.2 Catalyst characterization

The powder X-ray diffraction (XRD) patterns of the catalysts were recorded at room temperature with a Bruker AXS D8 Advance X-ray diffractometer operating at 45 kv and 200 mA with a radiation source of Cu Kα. The catalysts were scanned with a step size of 0.02° in the range of 10–80°, and the scan rate of 10°/min.

The N_2 adsorption-desorption isotherms were measured on 3H-2000PS2 surface aperture analyzer (Beishide Instrument Technology Corporation, China) at liquid nitrogen temperature (-196°C). The specific surface area and pore structure parameters were calculated by the Brunauer Emmett Teller (BET) method and the

Barrett-Joyner-Halenda (BJH) method, respectively. Before measurements, all samples were degassed under vacuum at 300°C for 4 h to remove physically adsorbed impurities.

Transmission electron microscopy (TEM), High-resolution TEM (HRTEM) and Energy-dispersive spectrometer (EDS) mapping observations used a FEI Talos F200X microscope with an acceleration voltage of 200 KV. Before testing, a suspension of the samples in ethanol was placed on a holey-carbon grid and then dried in air.

X-ray photoelectron spectroscopy (XPS) was performed on an ESCALAB 250Xi from Thermo Fisher with monochromatic Al Kα radiation. The binding energy values were calibrated on the basis of the C1s peak (284.8 eV).

Infrared (IR) spectra of the CO adsorption experiments were performed with an FTIR spectrometer (Bruker INVENIO S) equipped with a Harrick DRIFT cell and an MCT/A detector. The catalyst has been purged in N_2 at 200 °C for 30 min to eliminate a majority of residual intermediates. After the purging process, the catalyst was cooled down to 25 °C in N_2 atmosphere. The in-situ DRIFTS experiments of CO adsorption have been carried out in 10% CO/N_2 atmosphere at 25 °C, followed with a purging process in N_2.

NH_3 temperature programmed desorption (NH_3-TPD) were performed with an Autochem II 2920 analyzer (Micromeritics) equipped with a thermal conductivity detector (TCD). Before measurement, 0.1 g sample was pretreated for 1 h in He flow at 200 °C and then cooled to 25 °C. Thereafter, the sample was saturated with continuously 10 vol% NH_3/N_2. Finally, the sample was heated at a rate of 15 °C/min from 25 °C up to 800 °C in the 30 mL/min He.

H_2 temperature-programmed reduction (H_2-TPR) experiments were performed with an Autochem II 2920 analyzer (Micromeritics) equipped with a thermal conductivity

detector (TCD). 50 mg catalyst was pretreated in 30 ml/min of Ar at 300°C for 30 min to remove the adsorbed carbonates and hydrates. After cool down to room temperature, the catalyst was heated in 10% H_2/Ar (30 ml/min) from 40°C to 600°C with a heating rate of 10°C/min.

All of the in situ diffuse reflectance infrared Fourier transform spectroscopy (in situ DRIFTS) experiments were performed with an FTIR spectrometer (Bruker INVENIO S) equipped with a Harrick DRIFT cell and an MCT/A detector in the range of 650–8000 cm^{-1} with 32 scans at a resolution of 4 cm^{-1} using a KBr window. In a typical experiment, the powder samples were pre-treated in pure N_2 (100 mL min^{-1}) at 300 °C for 1 h to remove the residuals. After cooled down to 25 °C, the background spectrum was collected at 4 cm^{-1} resolution for 32 scans in N_2 atmosphere. And then the reactant gas (500 ppm toluene/N_2) with 100 mL min^{-1} was continuously introduced into the in situ reaction chamber. The DRIFTS spectra (4000–650 cm^{-1}) were collected and continuously recorded for 1 h to realize the adsorption equilibrium at different temperature (25, 100, 150, 200, 250 and 300 °C).

1.3 Catalytic activity evaluation

The catalytic performance evaluation experiments of toluene were carried out in a continuous fixed-bed reactor with 8 mm internal diameter and 350 mm in length at atmospheric pressure and a reaction temperature of 100–300°C. A K-type thermocouple was positioned in the catalyst bed to obtain accurate measurements of the catalyst temperature. The 0.2 g of catalyst (40-60 mesh) was mixed with 0.2 g of quartz to minimize the effect of possible hot spots, and both ends of the catalyst bed were fixed with quartz wool. Gaseous toluene was produced by N_2-bubbling in liquid toluene, and the sample was kept in a water bath at 20 °C. The total flow rate of the reactant mixture was 100 ml/min, which consisted of 1000 ppm toluene, 21% O_2, and

N_2 for the balance. The feed stream was controlled with mass-flow controller (MFC).

The toluene concentration of the inlet and exit gas stream was determined by on-line gas chromatography (GC-2014C, Shimadzu, Japan) equipped with a FID detector and the concentration of CO_2 in the exit was detected by an infrared gas analyzer (NK-500A, Xi'an Nuoke Instrument Co., Ltd, China). The toluene concentration ($X_{C_7H_8}$) and CO_2 yield (Y_{CO_2}) was calculated according to the following equations:

$$X_{C_7H_8} = \frac{[C_7H_8]_{in} - [C_7H_8]_{out}}{[C_7H_8]_{in}} \times 100\%$$

$$Y_{CO_2} = \frac{[CO_2]_{out}}{7[C_7H_8]_{in}} \times 100\%$$

Here, $[C_7H_8]_{in}$ and $[C_7H_8]_{out}$ refer to the inlet and exit concentration of toluene and $[CO_2]_{out}$ was the exit concentration of CO_2.

The turnover frequency (TOF, s^{-1}) and reaction rates (γ, mmol/g s) of the PCS and prepared catalysts according to the following formula:

$$TOF_{Pt\ or\ Mn}\ (s^{-1}) = C \cdot F \cdot X \frac{M_{Pt\ or\ Mn}}{m_{cat} X_{Pt\ or\ Mn} D_{Pt\ or\ Mn}} \quad (1)$$

$$\gamma = \frac{C \cdot F \cdot X}{m_{cat}} \quad (2)$$

where C is the toluene concentration (ppm), F is the total flow rate (ml/min), X is the toluene conversion, $M_{Pt\ or\ Mn}$ is the molar mass of Pt or Mn, $X_{Pt\ or\ Mn}$ is the weight fraction of Pt or Mn, $D_{Pt\ or\ Mn}$ is the disperison of Pt or Mn and m_{cat} represents the mass of the catalyst (g). (According to the available literature, it is difficult to accurately determine the actual dispersion of metals in such catalyst systems，thus we take the $D_{Pt\ or\ Mn}$ as 1.)

2. Results and Discussion

2.1 The toluene reaction rates

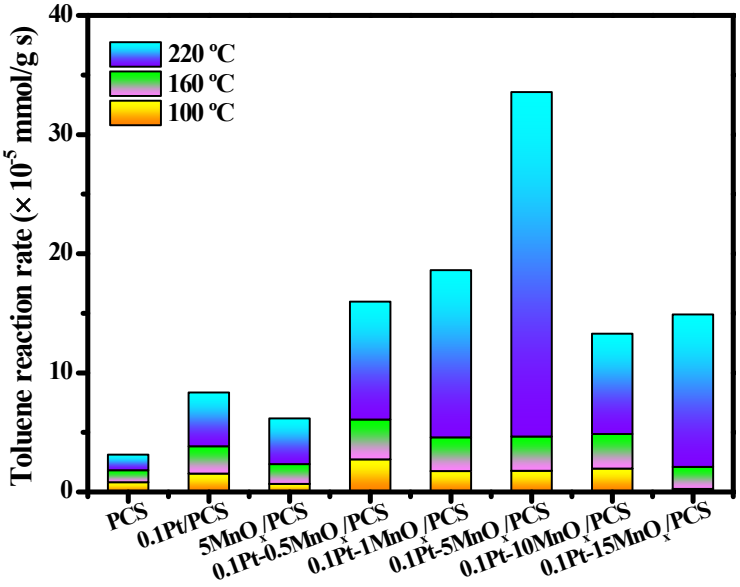

Fig. S1. The toluene reaction rates of the PCS and prepared catalysts at 100, 160 and 220 °C.

2.2 Structure and textural properties

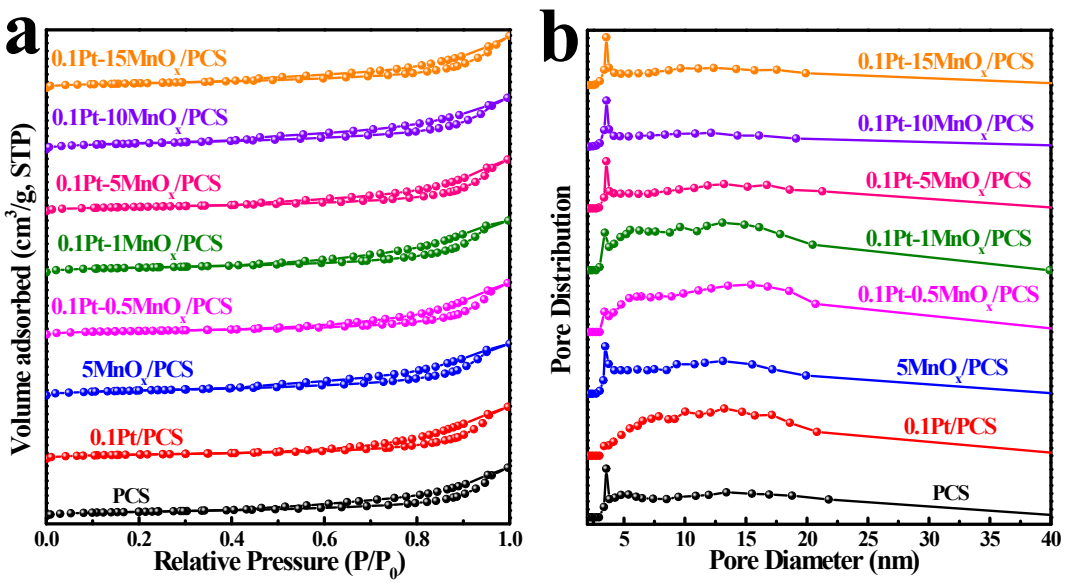

Fig. S2. N_2 adsorption-desorption isotherms (a) and corresponding BJH pore size distribution curves (b) of the PCS and prepared Pt-MnO_x/PCS catalysts

Table S1. BET surface area, average pore diameter and pore volume of the PCS and prepared Pt-MnO_x/PCS catalysts

Sample	S_{BET} (m^2/g)	D_{pore} (nm)	V_{pore} (cm^3/g)
PCS	143.3333	14.2047	0.5090
0.1Pt/PCS	129.3891	15.5036	0.5015
5MnO_x/PCS	123.7193	12.2212	0.3780
0.1Pt-0.5MnO_x/PCS	110.2057	16.2496	0.4477
0.1Pt-1MnO_x/PCS	126.4372	13.1544	0.4158
0.1Pt-5MnO_x/PCS	123.8531	14.5947	0.4519
0.1Pt-10MnO_x/PCS	119.6103	13.1962	0.3946
0.1Pt-15MnO_x/PCS	128.8347	13.5398	0.4361

Fig. S2 shows the N_2 adsorption-desorption isotherm and corresponding BJH pore size distribution of the PCS and prepared catalysts. All samples displayed a type II sorption isotherm with IUPAC H_3-type hysteresis loop in the P/P_0 range of 0.6-1.0 (**Fig. S2(a)**), indicating that there are many mesopores in the sample [S1]. The mesoporous structure of the support is conducive to the dispersion of the active components and reactants and promotes the rapid catalytic reaction [S2]. The textural properties of the catalysts are summarized in **Table S1**. We can see that the specific surface area of the PCS was 143.33 m^2/g, after loading Pt and MnO_x, the specific surface area of the catalysts decreased slightly, but the values was not related to the catalytic performance of toluene, which indicated that the specific surface area is not the crucial factor. Further, compared with the PCS, the pore diameter of the catalyst did not change significantly, concentrating around 12 to 16 nm, and the pore volume decreased slightly, which may be attributed to Pt and Mn blocking part of the pores of PCS.

References:

[S1] F.J. Liu, T. Willhammar, L. Wang, L.F. Zhu, Q. Sun, X.G. Meng, W. Carrillo-Cabrera, X.D. Zou, F.S. Xiao, J. Am. Chem. Soc, 2012, **134**, 4557-4560. https://doi.org/10.1021/ja300078q

[S2] F.J. Liu, S.F. Zuo, C. Wang, J.T. Li, F.S. Xiao, C.Z. Qi. Appl. Catal. B-Environ. 2014, **148-149**, 106-113. https://doi.org/10.1016/j.apcatb.2013.10.054

Table S2. Survey of literature on the catalytic oxidation of toluene

Catalyst	Reactant composition	T_{90} (°C)	Refs
Mn_3O_4	1000 ppm C_7H_8, 15000 mL/(g h)	270	[S3]
$15MnO_x/Al_2O_3$	1000 ppm C_7H_8, 21000/h	337	[S4]
1.0 Pt/TiO_2	975 ppm C_7H_8, 16000/h	212	[S5]
0.3Pt/MCM-41	500 ppm C_7H_8, 10000/h	195	[S6]
$0.31Pt/MnO_2$	500 ppm C_7H_8, 22500 mL/(g h)	164	[S7]
$0.39Pt/\gamma\text{-}MnO_2$	1000 ppm C_7H_8, 60000 mL/(g h)	190	[20]
$0.37Pt\text{-}MnO_2/CeO_2$	1000 ppm C_7H_8, 40000 mL/(g h)	218	[17]
$0.37Pt/MnO_2$	1500 ppm C_7H_8, 40000 mL/(g h)	250	[S8]
$0.2Pt/Mn_2O_3$	1000 ppm C_7H_8, 40000 mL/(g h)	253	[47]
0.23Pt/Mn/Bentonite	243 ppm C_7H_8, 12000/h	324	[S9]
$0.1Pt\text{-}5MnO_x/PCS$ (This work)	1000 ppm C_7H_8, 30000 mL/(g h)	237	--

[S3] S.C. Kim, W.G. Shim, Appl. Catal. B-Environ. 2010, **98**, 180-185. https://doi.org/10.1016/j.apcatb.2010.05.027

[S4] S.H. Xie, J.G. Deng, X.Y. Liu, Z.H. Zhang, H.G. Yang, Y. Jiang, H. Arandiyan, H.X. Dai, C.T. Au, App. Catal. A-Gen. 2015, **507**, 82-90. https://doi.org/10.1016/j.apcata.2015.09.026

[S5] V.P. Santos, S.A.C. Carabineiro, P.B. Tavares, M.F.R. Pereira, J.J.M. Órfão, J.L. Figueiredo, Appl. Catal. B-Environ. 2010, **99**, 198-205. https://doi.org/10.1016/j.apcatb.2010.06.020

[S6] X.R. Liu, Y. Liu, W.Y. Y, Z.B. Wu, Catal. Commun. 2016, **83**, 22-26. https://doi.org/10.1016/j.catcom.2016.05.001

[S7] X.X. Duan, Z.P. Qu, C. Dong, Y. Qin, Appl. Surf. Sci. 2020, **503**, 144161. https://doi.org/10.1016/j.apsusc.2019.144161

[20] S.P. Mo, Q. Zhang, M.Y. Zhang, Q. Zhang, J.Q. Li, M.L. Fu, J.L. Wu, P.R. Chen, D.Q. Ye, Nanoscale. Horiz. 2019, **4**, 1425-1433. https://doi.org/10.1039/C9NH00303G

[17] X.H. Fu, Y.X. Liu, J.G. Deng, L. Jing, X. Zhang, K.F. Zhang, Z. Han, X.Y. Jiang, H.X. Dai, Appl. Catal. A-Gen. 2020, **595**, 117509. https://doi.org/10.1016/j.apcata.2020.117509

[S8] J. Hu, X.L. Gao, Q.F. Fan, X.M. Gao, RSC. Adv. 2021, **11**, 16547-16556. https://doi.org/10.1039/D1RA02112E

[47] W.B. Pei, Y.X. Liu, J.G. Deng, K.F. Zhang, Z.Q. Hou, X.T. Zhao, H.X. Dai, Appl. Catal. B-Environ. 2019, **256**, 117814. https://doi.org/10.1016/j.apcatb.2019.117814
[S9] J. Esteban Colman-Lerner, M.A. Peluso, J.E. Sambeth, H.J. Thomas, React. Kinet. Mech. Cat. 2013, **108**, 443-458. http://dx.doi.org.10.1007/s11144-012-0525-2

Table S3. Assignment of IR bands appearing during the catalytic oxidation process of toluene at different temperature.

Position/cm^{-1}	Assignment	characteristic of
1308, 1337, 1361	δ(CH_2) deformation vibration	methylene (–CH_2) group
1435, 1491, 1591	skeletal υ(C=C) stretching vibration	aromatic ring
1535, 1546	υ(COO) stretching vibrations	benzoate or carboxylate species
1697, 1731, 1749	υ(C=O) stretching vibration of aldehyde	benzaldehyde
1828, 1843, 1866	υ(C=O) stretching vibration of anhydride	maleic anhydride
2326, 2381	υ(C=O) stretching vibration	carbon dioxide
2908, 2937	δ(CH_2) bending vibration	methylene (–CH_2) group
2985	δ(C-H) stretching vibrations	aromatic ring
3035	δ(C-H) stretching vibrations	methyl (–CH_3) group
3647	asymmetric υ(H-O) stretching vibrations	water